

Article

Comparison of Granites from the Eastern and Western Districts of the Gejiu Ore District in South China: Implication for Petrogenesis and Tin Metallogeny

Saijun Sun ^{1,2,*,†} , Junjie Zhang ^{1,2,3,†}, Shuang Li ^{4,*}, Haobin Niu ⁵, Zhaojian Wu ⁶ and Weidong Sun ^{1,2,3}

¹ Center of Deep Sea Research, Institute of Oceanology, Chinese Academy of Sciences, Qingdao 266071, China; zhangjunjie@qdio.ac.cn (J.Z.)

² Laboratory for Marine Geology, Laoshan Laboratory, Qingdao 266061, China

³ University of Chinese Academy of Sciences, Beijing 100049, China

⁴ Guangxi Key Laboratory of Hidden Metallic Ore Deposits Exploration, College of Earth Science, Guilin University of Technology, Guilin 541004, China

⁵ Chengdu Center, China Geological Survey, Chengdu 610081, China

⁶ Special Technology Exploration Center of China National Administration of Coal Geology, China Coal Geology Group Corporation Limited, Beijing 100040, China

* Correspondence: sunsaijun@qdio.ac.cn (S.S.); lishuang@glut.edu.cn (S.L.)

† These authors contributed equally to this work.

Abstract: Late Cretaceous granitoids are developed in the eastern and western districts of the Gejiu ore district, but tin deposits mainly occur in the eastern district, and the reasons for the difference in mineralization between the eastern and western districts are still controversial. Considering the main factors controlling granite Sn fertility, the whole-rock geochemical characteristics of granites on both sides are compared. LA-ICP-MS zircon U-Pb analyses of the Gejiu granites yielded two age periods: the early phase from 79.2 to 83.3 Ma and the later phase from 73.8 to 75.6 Ma. The western district granites have higher zircon $\epsilon_{\text{Hf}}(t)$, CaO/Na₂O, Ba, and Sr concentrations and lower Rb/Sr ratios than the eastern district granites, indicating that the western district granites have more mantle-derived materials in the source than the eastern district granites. Results of oxygen fugacity show that the western granites have a higher oxygen fugacity condition. More depleted Ba, Sr, P, Eu and Ti characteristics with obviously negative Eu anomalies in the eastern granites also have high Rb/Sr ratios and low Nb/Ta and Zr/Hf ratios, indicating that the eastern granites experienced highly magmatic differentiation, attributed to high volatile F contents that can reduce the viscosity and solidus of magma. Combined with the differences in field observations and structural styles, on the whole, the western district granites have higher oxygen fugacities and lower F contents and magmatic differentiation than those in the eastern district granites, indicating that the western district granites are not conducive to mineralization.

Keywords: Late Cretaceous granite; magma source; melting condition; biotite; Gejiu tin ore



Citation: Sun, S.; Zhang, J.; Li, S.; Niu, H.; Wu, Z.; Sun, W. Comparison of Granites from the Eastern and Western Districts of the Gejiu Ore District in South China: Implication for Petrogenesis and Tin Metallogeny. *Minerals* **2023**, *13*, 691. <https://doi.org/10.3390/min13050691>

Academic Editor: Aleksei V. Travin

Received: 3 April 2023

Revised: 11 May 2023

Accepted: 15 May 2023

Published: 19 May 2023



Copyright: © 2023 by the authors. Licensee MDPI, Basel, Switzerland. This article is an open access article distributed under the terms and conditions of the Creative Commons Attribution (CC BY) license (<https://creativecommons.org/licenses/by/4.0/>).

1. Introduction

As the main component of the Earth's continental crust, granite plays an important role in the evolution of the continental crust and the formation of many economic metallogenic belts [1–4]. Granite-related deposits are important sources of copper, molybdenum, tungsten and tin. Moreover, magmatic source, magmatic physicochemical property (P-T-fO₂) and evolution process (degree of magmatic fractionation) control the metallogenic potential of granitoids and their genetic relationship with certain types of ore deposits [5–7]. In general, porphyry Cu-Mo deposits are associated with oxidized magmas, while Sn-W deposits are related to reduced, high-fractionated felsic magmas [6–9]. Cretaceous granitoids are widely distributed in South China, and associated magmatic-hydrothermal deposits are also developed, which are important Cretaceous metallogenic areas in China. However, the mineralization of different ore-forming elements shows regional discrepancies, especially for tin mineralization.

The Gejiu tin polymetallic ore district, one of the largest mining districts in the world, is located in the western Cathaysia Block of South China [10–19] (Figure 1). The total ore reserves (including Sn, Cu, Pb, Zn, etc.) are more than 1000 Mt [20]. The Gejiu ore district contains two parts, eastern and western, divided by an N-S striking Gejiu fault (Figure 1c). Even though the late Cretaceous igneous rocks closely associated with the tin polymetallic mineralization are, in theory, widely distributed in both parts [10–14,16,18,19], most of the tin polymetallic deposits (Malage, Songshujiao, Gaosong, Laochang and Kafang deposits) are located in the eastern district, while only sporadic small Pb-Sn ore bodies occur in the western district [10–13,15,21,22]. This implies that other factors besides the magmatic sources also affect tin mineralization. However, few predecessors have studied the essential mechanism of the difference in mineralization distribution on both sides of the striking fault in the Gejiu area [22]. In this paper, considering the factors controlling the tin fertility of granites, a comprehensive study of Late Cretaceous granites from the Gejiu ore district has been taken to compare their geochemical characteristics with those of the eastern and western districts and further constrain the mineralization of the Gejiu Sn district.

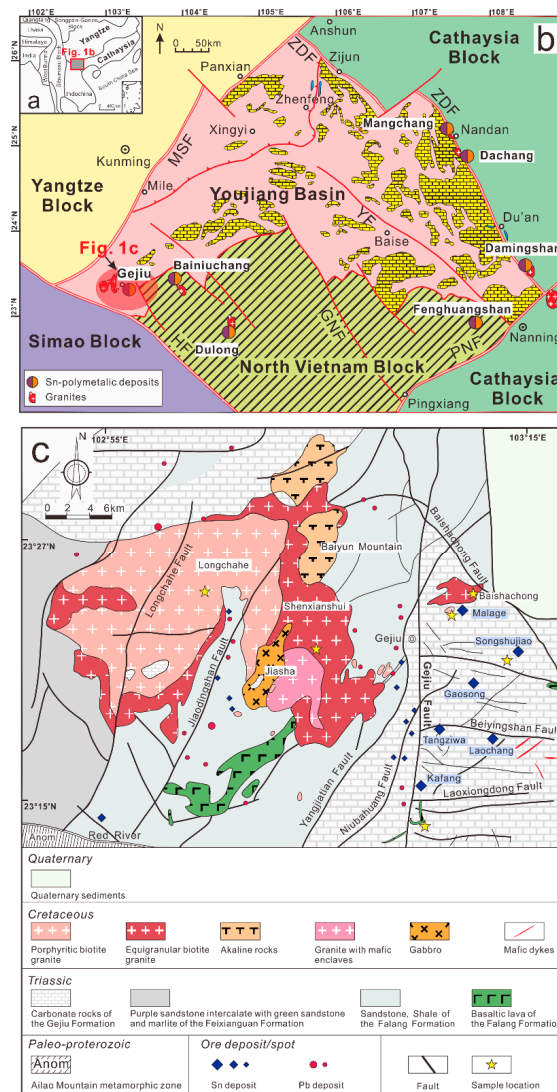


Figure 1. (a) Simplified map of main tectonic units in East Asia (modified after [16]). (b) Simplified geological map of Youjiang Basin displaying the distribution of late Cretaceous granitic rocks and related ore deposits (modified from [13,18]). (c) Simplified geological map of the Gejiu ore district (modified from [13,18]). ZDF, Ziyun–Du’an fault zone; PNF, Pingxiang–Nanling fault zone; HF, Honghe fault zone; MSF, Mile–Shizong fault zone.

2. Geological Setting and Sample Description

The Gejiu tin polymetallic ore district is located near the southwestern margin of the South China Block, which experienced multi-stage arc magmatic activities related to paleo-Pacific or Tethys plate subduction [10–14,18,23–26]. Several stages of back-arc crustal extension related to the reorganization of the subduction zone formed the main tin and tungsten mineralization. The Gejiu ore district is located near the city of Gejiu and is bounded by the Yangtze Block to the north and by the Sanjiang fold belt to the west (Figure 1a,b). It occupies about 1600 km², and the strata in this district range from Cambrian to Quaternary. The Late Triassic to Cretaceous strata are exposed due to the Yanshanian tectonic movement [15]. The Middle Triassic Gejiu Formation and the Middle Triassic Falang Formation are the main outcrops in this area. The Gejiu Formation is mainly composed of carbonate (>3000 m thick), which is the host rock of the deposit in the Gejiu area. The Falang Formation is mainly composed of clastic sediments and carbonate with interlayered mafic lavas (1800 to 2800 m thick) [10–13]. Faults are well developed in the Gejiu area, including the NNE-trending Longchahe faults, NE-trending Baishachong fault and NS-trending Gejiu fault [11].

The Gejiu fault cuts through the whole district, and divides it into eastern and western parts (Figure 1c). Most of the tin polymetallic deposits are located in the eastern part, including the Malage, Songshujiao, Gaosong, Laochang, and Kafang deposits [11]. The Gejiu granite is one of the largest batholiths in the western Cathaysia Block. Igneous rocks in the eastern district are mainly concealed, including Baichachong, Malage–Songshujiao, and Laochang–Kafang granitic intrusions, with few outcropped rocks in Baishachong, Beipaotai, and Kafang areas [27] (Figure 1c). Igneous rocks in the western district are mainly outcropped, including mafic, acidic and alkaline rocks, but the granite formed during Yanshanian is dominant. Moreover, the Longchahe, Shenxiangshui granitic, and Jiasha gabbro intrusions are located in the western district (Figure 1c). Granitic rocks in the Gejiu area can be divided into two types: porphyritic and equigranular [10,13]. Granitic rocks from Longchahe and Malage–Songshujiao intrusions belong to the porphyritic type, while granitic rocks from Baishachong, Shenxiangshui, and Laochang–Kafang intrusions belong to the equigranular type. The Jiasha intrusion is composed of gabbro and monzonite.

Numerous granite samples were collected from the Gejiu area (Figure 2). The phenocryst content of the porphyritic granite from Longchahe and Malage–Songshujiao intrusions is about 40%, and grains consist of plagioclase, K-feldspar, quartz, and biotite (Figure 2a–c). The groundmass is mainly comprised of plagioclase, K-feldspar, quartz, and biotite, with minor accessory minerals, e.g., zircon, apatite, and titanite (<5%). The plagioclase (~30%) has polysynthetic twins, with sericite alteration in some samples. The K-feldspar (~30%) consists of orthoclase, microcline, and perthite. The microcline has typical crosshatched twins, and the perthite has perthitic textures. Quartz (~25%) grains appear subhedral or anhedral. The biotite (~10%) shows chloritization and muscovite alteration in some samples. The equigranular granites from Baishachong, Shenxiangshui, and Laochang–Kafang intrusions include plagioclase (35%), K-feldspar (25%), quartz (25%), and abundant biotite (10%), with minor accessory minerals, e.g., zircon and titanite (<5%) (Figure 2d–f).

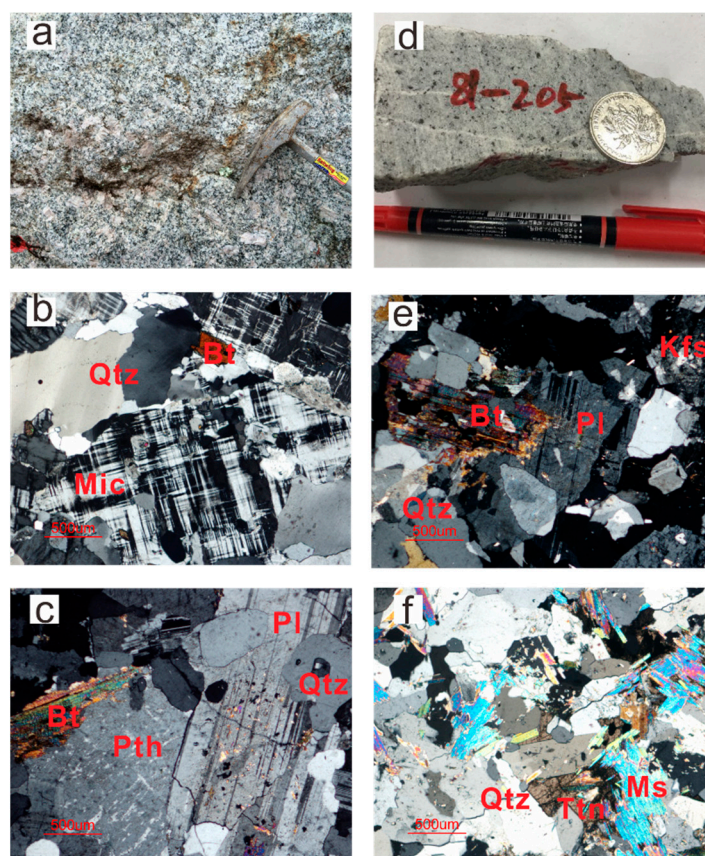


Figure 2. Hand specimen photographs and photomicrographs of porphyritic granites (a–c) and equigranular granites (d–f) from the Gejiu ore district. Bt, biotite; Kfs, K-feldspar; Mic, microcline; Ms, muscovite; Pl, plagioclase; Pth, perthite; Qtz, quartz; Ttn, titanite.

3. Analytical Methods

3.1. Major and Trace Elements of Whole Rocks

Major and trace element (including rare earth elements (REE)) concentrations were analyzed for whole-rock samples at the State Key Laboratory of Isotope Geochemistry of the Guangzhou Institute of Geochemistry, Chinese Academy of Sciences (SKLIG-GIGCAS). The detailed analytical methods were described by Li et al. [28].

For major element analysis, a devolatilized or ignited sample (~0.6 g) was added to lithium borate flux (~4.8 g, $\text{Li}_2\text{B}_4\text{O}_7$), mixed well, and fused in an auto fluxer at a temperature of 1250 °C. It was then cooled to form a flat molten glass disc, which was then analyzed by a Rigaku 100e X-ray fluorescence spectrometer. Analytical uncertainties were better than 1%. Trace elements were analyzed by a Perkin-Elmer ELAN 6000 ICP-MS. The REEs were analyzed by cation exchange separation-inductively coupled plasma atomic emission spectrometry (ICP-AES). The analytical precision and accuracy of trace elements were better than 5%.

3.2. Zircon U-Pb Dating

Zircons were separated from the granite samples using magnetic and heavy liquid separation methods and were then purified by handpicking under the binocular microscope. Approximately 100 zircon grains were mounted on an adhesive tape, enclosed in epoxy resin, polished, and then photographed under both transmitted and reflected light. The internal structures of the zircons were examined using the cathodoluminescence (CL) imaging technique at the Analytical Center of the University of Science and Technology of China. The U-Pb isotopic ratios of zircons were analyzed by an Agilent 7500a ICP-MS coupled with a RESOLUTION M-50 laser ablation system at the Guangzhou Institute of Geochemistry,

Chinese Academy of Science (GIG.CAS), following the procedures outlined by [6,23,24,29]. The spot size of the laser beam was set at $\sim 31 \mu\text{m}$. Off-line inspection and integration of background and analytical signals, time-drift correction, and quantitative calibration for trace element analyses and U-Pb dating were performed using ICPMSDataCal [30]. The U-Pb ages of zircons were calculated using the ISOPLOT program [31].

3.3. In-Situ Zircon Hf Isotopes

In-situ zircon Hf isotope analyses were conducted on the U-Pb-dated spots using a RESOLUTION M-50 laser ablation system attached to a Thermo Finnigan Neptune MC-ICP-MS at the GIG.CAS. The laser-ablated spot size was $44 \mu\text{m}$. The natural Penglai zircon megacrysts were used as the reference material [32]. The detailed instrumental parameters and analytical techniques are the same as reported by [23,29]. The mass fractionations of Hf were calculated with a reported 0.7325 for $^{179}\text{Hf}/^{177}\text{Hf}$ [32]. The isobaric correction of ^{176}Lu on ^{176}Hf used the isotopic ratios of $^{176}\text{Lu}/^{175}\text{Lu} = 0.02655$ and $^{176}\text{Yb}/^{172}\text{Yb} = 0.5887$ during analysis [30,33].

3.4. Mica Compositions

Major elements of micas were determined by using a wavelength-dispersive JEOL JXA-8230 electron microprobe (EMP) at the Instrumental Analysis and Research Center, Guilin University of Technology. The analysis was made with an accelerating voltage of 15 kV and a beam current of 2×10^{-8} A. The diameter of the electron beam was $5 \mu\text{m}$. The calibration was based on a suite of mineral and oxide standards from the American Standard Committee [34].

4. Results

4.1. Major and Trace Elements of Whole Rocks

The major and trace element compositions of granites from the Gejiu area are listed in Table S1. The granite samples range from 64.2 to 76.6 wt.% SiO_2 , 12.9 to 16.2 wt.% Al_2O_3 , 4.00 to 5.80 wt.% K_2O , and 7.49 to 8.55 wt.% total alkali content ($\text{K}_2\text{O} + \text{Na}_2\text{O}$) (Table S1). They show $\text{Mg}^\#$ values from 10.7 to 39.5 and 1.01 to 2.44 for $\text{K}_2\text{O}/\text{Na}_2\text{O}$ ratios and belong to the calc-alkaline and shoshonite series (Figure 3a). They also show a peraluminous character, with the alumina saturation index A/CNK varying from 1.01 to 1.24 (Table S1). The Longchahe granite samples (western sector) from [10] have A/CNK ratios from 0.76 to 1.05, and most of these samples are metaluminous. The Laochang–Kafang granite samples (eastern sector) from [10] show A/CNK values from 1.02 to 1.15, belonging to peraluminous.

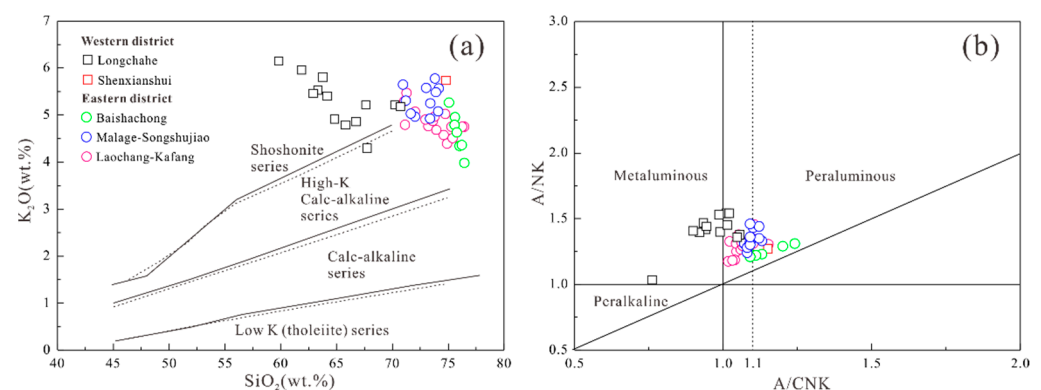


Figure 3. (a) SiO_2 vs. K_2O diagram of the granites from the Gejiu ore district. (b) A/NK vs. A/CNK diagram of granites from the Gejiu ore district. $\text{A/NK} = \text{Al}_2\text{O}_3/(\text{Na}_2\text{O} + \text{K}_2\text{O})$ (molar ratio), $\text{A/CNK} = \text{Al}_2\text{O}_3/(\text{CaO} + \text{Na}_2\text{O} + \text{K}_2\text{O})$ (molar ratio).

The primitive mantle normalized spider diagram shows that Gejiu granites are characterized by relative enrichments in Rb, Th, and U and depletions in Ba, Nb, P, Ti, and

Zr (Figure 4a). However, granites from the eastern district show stronger anomalies than those from the western district. Granites from the western district have relatively high REE contents, with the Σ REE values ranging from 173 to 560 ppm, while granites from the eastern district have relatively low REE contents, with the Σ REE values ranging from 101 to 314 ppm (Table S1). The chondrite-normalized REE patterns for all granite samples (Figure 4b) exhibit obvious fractionation between light rare earth elements (LREEs) and heavy rare earth elements (HREEs), with ratios of Σ LREE/ Σ HREE and La_N/Yb_N ranging from 1.36 to 32.1 and 0.82 to 66.1, respectively. The granites from the eastern district (Baishachong, Malage–Songshujiao, and Laochang–Kafang intrusions) show more strongly negative Eu anomalies with δ Eu values from 0.04 to 0.40 than those from the western district (Longchahe and Shenxianshui intrusions) from 0.63 to 0.88.

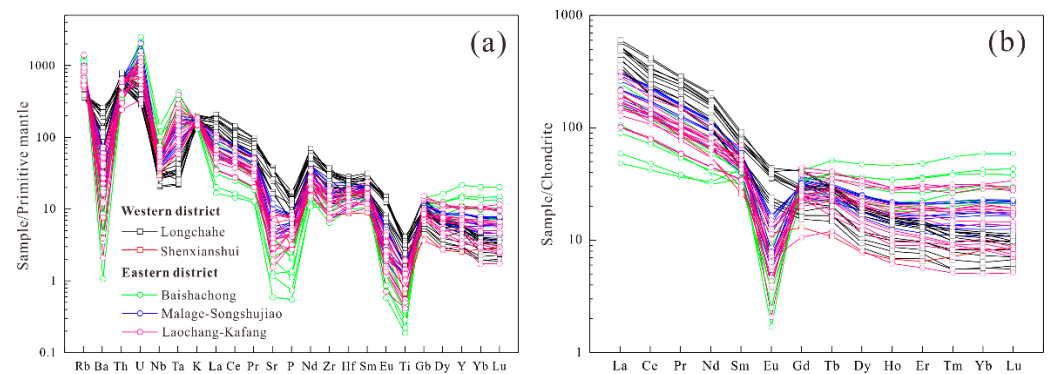


Figure 4. Distributions of trace elements and REEs of granite from the Gejiu ore district [35]. (a) Spider diagram of trace elements; (b) Chondrite-normalized REE patterns.

4.2. Zircon U-Pb Geochronology and Chemical Compositions

Zircon samples from six granite intrusions in the Gejiu ore district (LCH81–185 and SXS81–198 from the western district; SSJ81–205, BSC81–216, KF81–238, and MLG81–274 from the eastern district) are transparent and mainly euhedral in morphology, ranging from 50 to 200 μ m in diameter. The CL images show concentric oscillatory zoning (Figure S1), indicating their magmatic origin [36]. The zircon U-Pb dating data and chemical composition are reported in Table S2.

As regards the western district, 26 zircons of the Longchahe granite (LCH81–185) have high Th (76.6–1574 ppm) and U (429–4590 ppm) concentrations, with Th/U ratios ranging from 0.10 to 1.88 (Table S2). The data cluster in two groups on the Concordia diagram, one with a weighted mean $^{206}\text{Pb}/^{238}\text{U}$ age of 83.3 ± 0.98 Ma and the other with a weighted mean age of 75.6 ± 1.4 Ma (Figure 5a). Zircon Σ REE contents range from 266 to 1007 ppm, with the ratios of LREE/HREE ranging from 0.03 to 0.10 (Table S2). The δ Eu and δ Ce of these zircons range from 0.13 to 0.46 and from 3.74 to 315, respectively, showing negative Eu anomalies and strongly positive Ce anomalies (Figure S2a, Table S2).

Twenty-three zircons of the Shenxianshui granite (SXS81–198) in the western district have high Th (349–4069 ppm) and U (378–20,771 ppm) concentrations, with Th/U ratios ranging from 0.13 to 1.35 (Table S2). They yield a weighted mean $^{206}\text{Pb}/^{238}\text{U}$ age of 82.9 ± 1.3 Ma (Figure 5b). Zircon Σ REE content range from 510 to 2473 ppm, with LREE/HREE ratios ranging from 0.01 to 0.11, and their δ Eu and δ Ce range from 0.07 to 0.40 and from 4.94 to 43.6, respectively, showing negative Eu anomalies and strongly positive Ce anomalies (Figure S2b, Table S2).

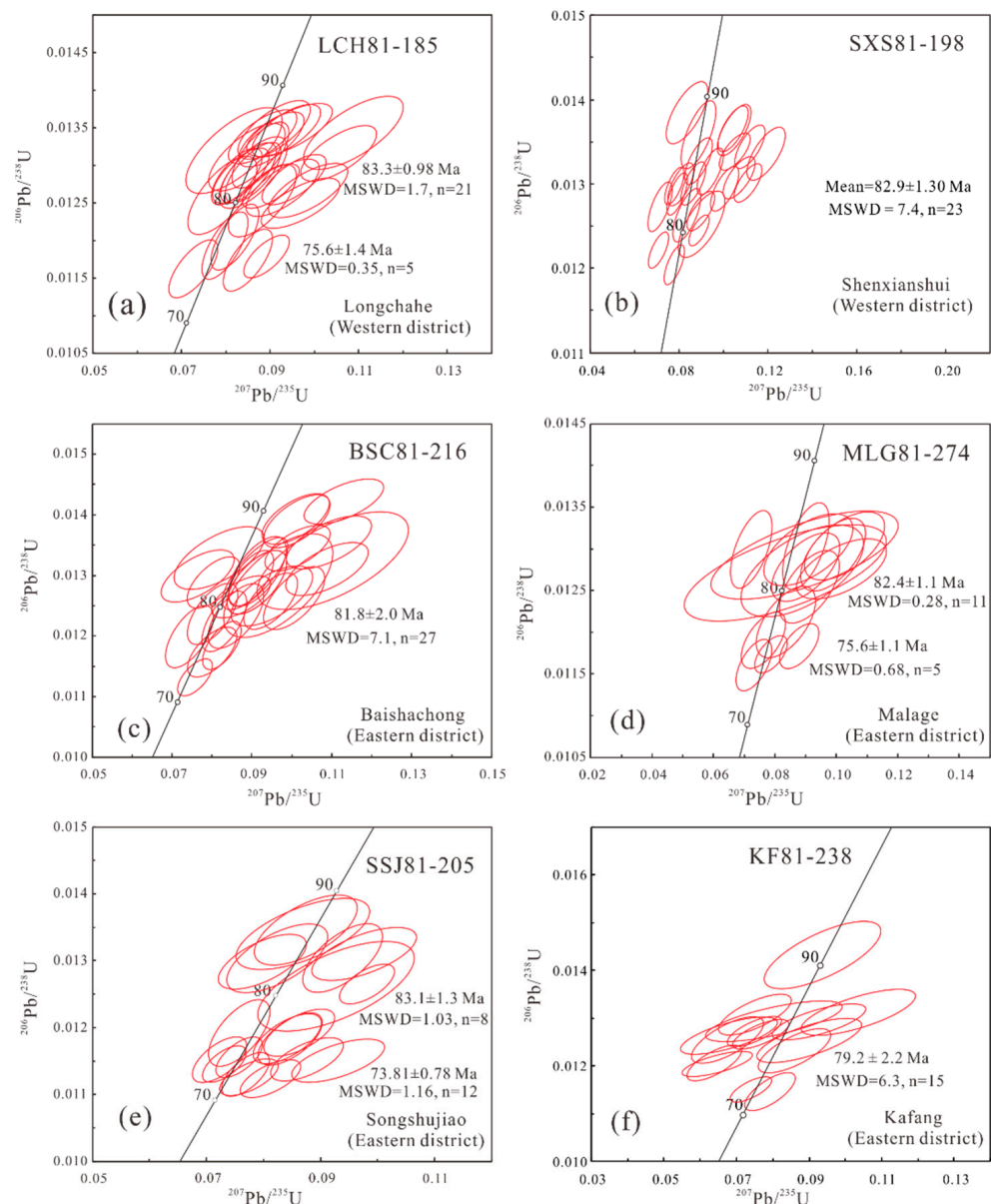


Figure 5. Concordia diagrams for zircons U-Pb ages ($^{206}\text{Pb}/^{238}\text{U}$ -weighted average ages) from the (a) Longchahe, (b) Shenxianshui, (c) Baishachong, (d) Malage, (e) Songshujiao, (f) Kafang granite in the Gejiu ore district.

As for the eastern district, 27 zircons of the Baishachong granite (BSC81–216) have high Th (101–17,519 ppm) and U (159–3656 ppm) concentrations, with Th/U ratios of 0.56–5.51 (Table S2). They yield a weighted mean $^{206}\text{Pb}/^{238}\text{U}$ age of 81.8 ± 2.0 Ma (Figure 5c). Zircon ΣREE contents range from 348 to 918 ppm, with variable LREE/HREE ratios (0.54–1.32) (Table S2), and their δEu and δCe range from 0.83 to 0.94 and from 8.16 to 76.5, respectively, showing slightly negative Eu anomalies and strongly positive Ce anomalies (Figure S2c, Table S2), indicating that the crystallization of zircons may be earlier than or simultaneous with plagioclase.

Sixteen zircons of the Malage granite (MLG81–274) in the eastern district have high Th (189 to 928 ppm) and U (349 to 5943 ppm) concentrations, with Th/U ratios ranging from 0.13 to 0.77 (Table S2). The data cluster in two groups on the Concordia diagram, one with a weighted mean $^{206}\text{Pb}/^{238}\text{U}$ age of 82.4 ± 1.1 Ma, and the other with a weighted mean age of 75.6 ± 1.1 Ma (Figure 5d). Zircon ΣREE contents range from 345 to 1137 ppm with variable ratios of LREE/HREE (0.01–0.05) and their δEu and δCe range from 0.01 to 0.18

and from 3.52 to 341.56, respectively, showing negative Eu anomalies and strongly positive Ce anomalies (Figure S2d, Table S2).

Twenty zircons of the Songshujiao granite (SSJ81–205) in the eastern district have high Th (188 to 873 ppm) and U (219 to 6778 ppm) concentrations, with Th/U ratios of 0.10 to 0.93 (Table S2). The data cluster in two groups on the Concordia diagram, one with a weighted mean $^{206}\text{Pb}/^{238}\text{U}$ age of 83.1 ± 1.3 Ma, and the other with a weighted mean age of 73.8 ± 0.78 Ma (Figure 5e). Zircon ΣREE contents range from 447 to 976 ppm, with LREE/HREE ratios ranging from 0.01 to 0.05, and their δEu and δCe range from 0.05 to 0.23 and from 3.20 to 113.23, respectively, showing negative Eu anomalies and strongly positive Ce anomalies (Figure S2e, Table S2).

Fifteen zircons of the Kafang granite (KF81–238) in the eastern district have high Th (219–2104 ppm) and U (440–6769 ppm) concentrations, with Th/U ratios of 0.18–1.30 (Table S2). They yield a weighted mean $^{206}\text{Pb}/^{238}\text{U}$ age of 79.2 ± 2.2 Ma (Figure 5f). Zircon ΣREE contents range from 404 to 1864 ppm, with LREE/HREE ratios ranging from 0.02 to 0.06, and their δEu and δCe range from 0.04 to 0.15 and from 1.91 to 666, respectively, showing negative Eu anomalies and strongly positive Ce anomalies (Figure S2f, Table S2).

Zircon $\text{Ce}^{4+}/\text{Ce}^{3+}$ ratios are listed in Table S2 [37]. The calculated zircon $\text{Ce}^{4+}/\text{Ce}^{3+}$ ratios of the Longchahe granite (LCH81–185) and Shenxianshui granite (SXS81–198) in the western district range from 39.7 to 286, from 2.11 to 101, respectively (Table S2). The calculated zircon $\text{Ce}^{4+}/\text{Ce}^{3+}$ ratios of the Songshujiao granite (SSJ81–205), Baishachong granite (BSC81–216), Kafang granite (KF81–238), and Malage granite (MLG81–274) range from 2.98 to 149, 0.79 to 5.19, 1.03 to 39.1, and 23.8 to 178, respectively (Table S2).

4.3. Zircon Lu-Hf Isotope Composition

Zircon samples from four granite intrusions in the Gejiu ore district (SXS81–198 from the western district; SSJ81–205, KF81–238, and MLG81–274 from the eastern district) were analyzed for their Hf isotopic composition, and their results are reported in Table S3.

As for the western district, 26 dated zircons of the Shenxianshui granite (SXS81–198) exhibit $\varepsilon_{\text{Hf}}(t)$ values from -8.3 to $+0.03$, with corresponding two-stage Hf model ages ranging from 979 to 1406 Ma. As for the eastern district, 20 dated zircons of the Songshujiao granite (SSJ81–205) exhibit $\varepsilon_{\text{Hf}}(t)$ values from -10.7 to -5.8 and the corresponding two-stage Hf model age is from 1270 to 1523 Ma. Fifteen dated zircons of the Kafang granite (KF81–238) exhibit $\varepsilon_{\text{Hf}}(t)$ values from -10.5 to -6.9 , with corresponding two-stage Hf model ages ranging from 1327 to 1517 Ma. Sixteen dated zircons of the Malage granite (MLG81–274) exhibit $\varepsilon_{\text{Hf}}(t)$ values from -9.5 to -5.7 and the corresponding two-stage Hf model age is from 1271 to 1472 Ma.

4.4. Mica Composition

The chemical compositions of micas from the granite in the Gejiu ore district are listed in Table S4. According to the $\text{Mg}-(\text{Fe}^{2+} + \text{Mn})-(\text{Fe}^{3+} + \text{Al}^{\text{VI}} + \text{Ti})$ diagram (Figure 6a), the biotite grains from the Longchahe granite are classified as magnesian biotite, while those from the Malage granite are ferro-biotite [38]. The biotite grains from the Longchahe granite have high MgO and FeO contents of 10.5–11.4 wt.% and 20.5–22.5 wt.%, respectively, and moderate Al_2O_3 contents of 14.3–15.0 wt.% with X_{Mg} values ($\text{Mg}/(\text{Mg} + \text{Fe})$) from 0.45 to 0.49 (Table S4). The biotite grains from the Malage granite have high FeO contents (25.3–34.0 wt.%) and relatively low Al_2O_3 (4.25–15.0 wt.%) and MgO (4.25–7.51 wt.%) contents with X_{Mg} values from 0.20 to 0.35 (Table S4).

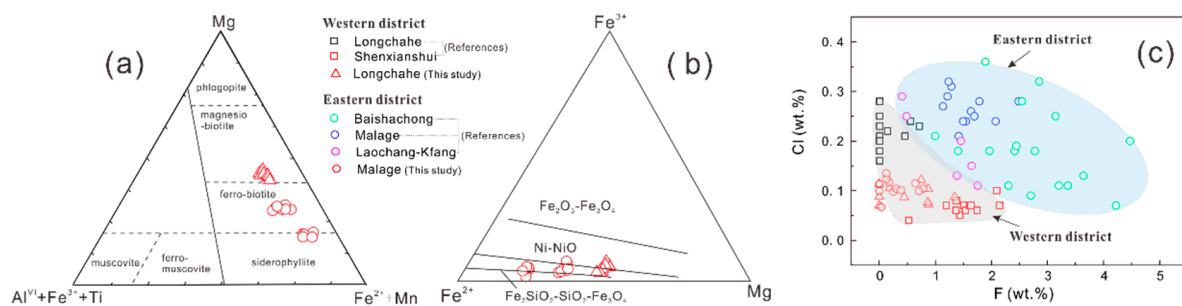


Figure 6. (a) Classification of biotite in the Gejiu ore district (after [37,38]). (b) Diagram of Fe^{3+} - Fe^{2+} -Mg for biotite from granites in the Gejiu ore district [39]. (c) F vs. Cl diagram of biotite in the Gejiu ore district. Reference data come from [40].

5. Discussion

5.1. Geochronology of the Gejiu Igneous Rocks

According to the in-situ dating of cassiterite in the metallogenic stage of the Gejiu ore district, the metallogenic age is 83–85 Ma, which is closely associated with the Late Cretaceous granitic plutons [14,17,41]. In this study, systematic LA-ICP-MS zircon U-Pb dating for six samples of granite from the east and west sides of the Gejiu Fault in the Gejiu ore district yielded two-period ages: the younger from 73.8 to 75.6 Ma and the older from 79.2 to 83.3 Ma, both belonging to the Late Cretaceous (Figure 5). However, this is slightly different from the previous zircon U-Pb ages analyzed by SHRIMP, SIMS, or LA-ICP-MS, which range from 76 Ma to 85 Ma [10–13,19]. We have identified a younger phase of magmatic activity (73.8–75.6 Ma). Previous data reported that Gejiu ore-forming processes involved ~94 Ma batholithic biotite monzogranites and ~72 Ma satellitic muscovite alkali-feldspar granites [42]. Furthermore, they suggested that both types of rocks were two stages of magmatic activity derived from a long-lived magma chamber. Regardless of whether the above is the case or not, it shows that there is still a stage of small-scale magmatic activity in the Gejiu ore district after the main metallogenic stage, which is consistent with the 73.8–75.6 Ma magmatic activity that we have identified.

5.2. Comparison of Metallogenic Differences between the Eastern and Western Districts in the Gejiu Ore District

The ore-controlling factors related to granitic rocks generally include the magmatic source or sources of ore-forming elements, their transportation and enrichment conditions, and their precipitation and mineralization mechanisms. Previous studies have shown that the main factors controlling granite Sn-W fertility are the magmatic source (ore-forming elements, volatiles, etc.), partial melting conditions (T - fO_2 , etc.), and magmatic differentiation [26,43–45]. Therefore, these factors are of great potential significance in revealing the reasons for the metallogenic difference between the east and west sides of the Gejiu district and in exploring the mineralization potential of other granites.

5.2.1. Magma Source

Previous studies proposed that the Gejiu Sn-polymetallic ore district is related to the Late Cretaceous granites [12,14,17,41]. These granites share a related genesis, but their metallogenic capacities are quite different [20,22]. Some studies suggest that these granites are derived from different magma sources, and others suggest that they come from different evolution stages of the same magmatic system [10–13,42]. Thus, whether the nature of the magmatic source controls the relationship between Late Cretaceous granites and their metallogenic capacities is still debated.

Based on the Nd-Pb-Hf-O isotope study, it is believed that the western and eastern Late Cretaceous granites in the Gejiu ore district shared similar magma sources, which originated from the Mesoproterozoic basement of the Yangtze Block [10,22,41]. However, our zircon $\varepsilon_{Hf}(t)$ values (−8.32 to +0.03) and previous data of the western district Gejiu

granite are slightly higher than those of the eastern district granite, which are from -10.7 to -5.7 (Table S3, Figure 7a,b), suggesting they have different melt sources. The western district granites appear to contain more mantle-derived materials in the magma source than the eastern district granites. The corresponding two-stage Hf model ages also have different distribution ranges (Figure 7c,d), in which the western district granites plot the range of the Late Mesoproterozoic period while the eastern district granites plot the range of the Early Mesoproterozoic period. This significant difference is consistent with literature data indicating that the granitoids from the western district have higher $\epsilon_{\text{Nd}}(t)$ values than those of the eastern district granites [10].

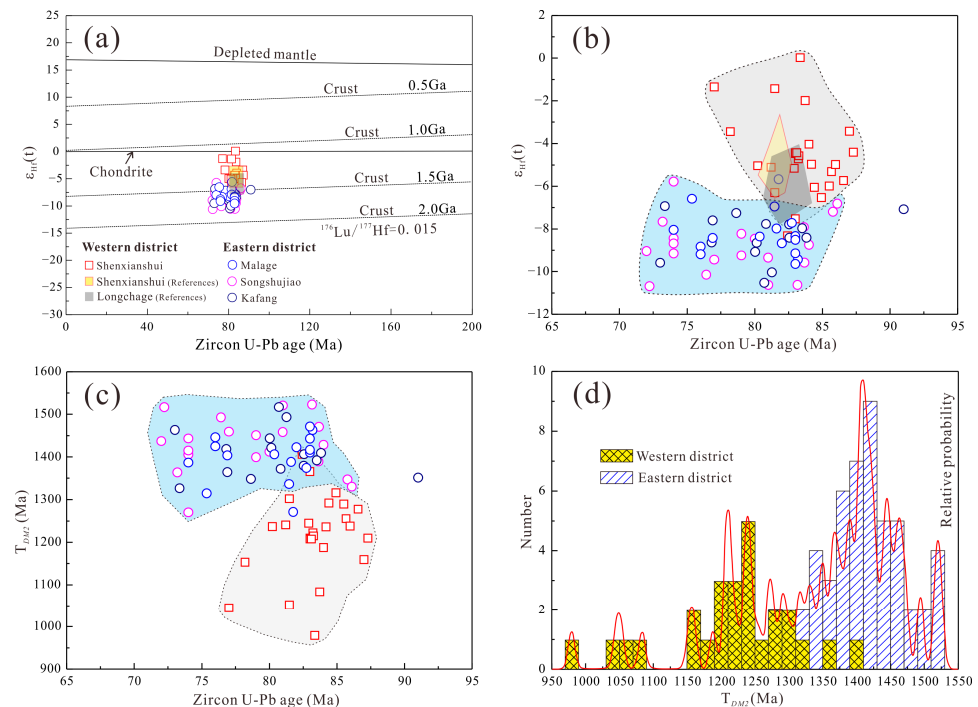


Figure 7. (a,b) $\epsilon_{\text{Hf}}(t)$ vs. U–Pb age diagram of zircons in the Gejiu ore district. (c) T_{DM2} vs. zircons U–Pb age in the Gejiu ore district. (d) Probability of Hf model age of zircons in the Gejiu ore district. Reference data come from [22].

We also find this difference in the major and trace element data. Typical crustal granites usually have relatively low Sr content (<300 ppm) [46,47], while the source of granite that contains mantle components will have high Sr and Ba concentrations [46,48,49]. Our granites from the western district (Longchahe and Shenxianshui intrusions) and previous data [10] show high Ba and Sr concentrations, ranging from 345 to 1830 ppm and 195 to 805 ppm, respectively, and relatively low Rb concentrations, ranging from 226 to 425 ppm (Table S1). The granites from the eastern district (Baishachong, Malage–Songshujiao, and Laochang–Kafang intrusions) show lower Ba and Sr concentrations, ranging from 7.49 to 513 ppm and 12.5 to 254 ppm, respectively, and higher Rb concentrations, ranging from 313 to 891 ppm (Table S1). This suggests the source of granites from the western district should contain more mantle components, while the granites from the eastern district should have a more crustal source, indicating magmatic sources may be important in controlling the Gejiu tin deposit.

Compared to the granites from the western district, those rocks from the eastern district show lower CaO/Na₂O ratios and higher Rb/Sr and Rb/Ba ratios (Figure 8), which are similar to the geochemical features of Permian–Triassic tin-bearing granites in the eastern and western belts of Peninsular Malaysia [41,50]. On the whole, granites from the eastern district display affinity for melts derived from clay-rich metapelitic sources, while those rocks from the western district could originate from the partial melting of clay-poor metagraywacke sources (Figure 8). According to the previous study [51], the

average Sn content of the tin-bearing granites from the eastern district (Baishachong, Malage-Songshujiao, and Laochang-Kafang intrusions) ranges from 22 to 29.8 ppm [9,52]. However, the average Sn content of the granites from the western district (Longchahe and Shexianshui intrusions) ranges from 1.15 to 13.97 ppm [51] (Table S1), thus the low Sn content in these granites might not be conducive to the formation of a tin deposit. Therefore, the western and eastern sources for the Gejiu granitic batholith may be different, and the western district granites may be derived from more mantle-derived melts and clay-poor metagraywacke sources compared with the eastern district granites.

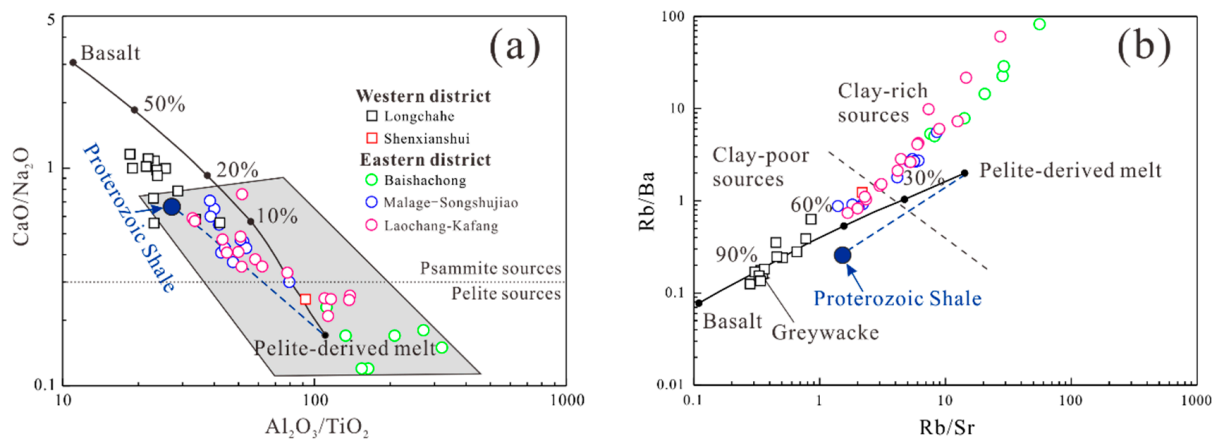


Figure 8. Whole-rock CaO/Na₂O vs. Al₂O₃/TiO₂ (a), and Rb/Ba vs. Rb/Sr ratios (b). The diagrams are modified after [53].

5.2.2. Melting Conditions

Tin has moderate incompatibility, so it is generally preferentially partitioned in the melt phase [54]. In addition to the importance of the enrichment of ore-forming elements in magmatic sources, partial melting conditions also play an important role in the enrichment of ore-forming elements [55,56].

Magma Redox State

Oxygen fugacity plays a key role in determining the ore-forming potential of plutonic bodies [57,58]. On the one hand, it controls the occurrence of variable elements in the magmatic system; on the other hand, these elements have a strong influence on the redox conditions of the magmatic system. Therefore, the redox state of magmas is commonly associated with different types of mineralization [6,24,25,56,58]. Tin has two dominant valence states (Sn²⁺ and Sn⁴⁺). At low oxygen fugacity, tin exists in the form of Sn²⁺ with incompatible behavior, becoming enriched in residual magma [4]. However, tin exists as Sn⁴⁺ at high oxygen fugacity with compatible behavior and incorporates early crystalline titanium-bearing minerals such as biotite, magnetite, and ilmenite, becoming depleted in residual magma [58,59]. And the transition from Sn²⁺-dominant valence to Sn⁴⁺-dominant valence occurs in the narrow range of fO_2 (FMQ = 1.0~2.0) [4,55]. Therefore, the redox state of magma is generally considered to be a key parameter for the genesis of tin deposits [4,55].

The Ce⁴⁺/Ce³⁺ and δEu values of zircon are good indicators of oxygen fugacity of the magmas producing tin granites [6,22–24,26,28,29,43]. In Figure 9, the majority of the western district granites have a higher oxygen fugacity than the eastern district granites. The chemical composition of biotite can also reflect oxidation conditions during magma crystallization. The concentrations of Fe³⁺, Fe²⁺, and Mg²⁺ in biotite, which is paragenetic with K-feldspar and magnetite, can be used to calculate the magmatic oxygen fugacity [28,39,60,61]. The Fe³⁺-Fe²⁺-Mg diagram shows biotites from the western granites were plotted between the HM and FMQ buffer lines, while biotites from the eastern granites were plotted between the NNO and FMQ (Figure 6b), indicating the western granites have a higher oxygen fugacity condition [61]. Generally, pelites, such as shale, are reduced in nature, and their oxygen fugacities are significantly lower than those of FMQ buffers [62].

Figure 8 shows that the eastern granites plot in a field of melts derived from a clay-rich metapelitic source, suggesting that the reduced oxidation state might be inherited from the pelitic source. The above results suggest that the western and eastern granites are derived from magmas with different oxygen fugacity, with the western district granites having a higher oxygen fugacity compared with the eastern granites.

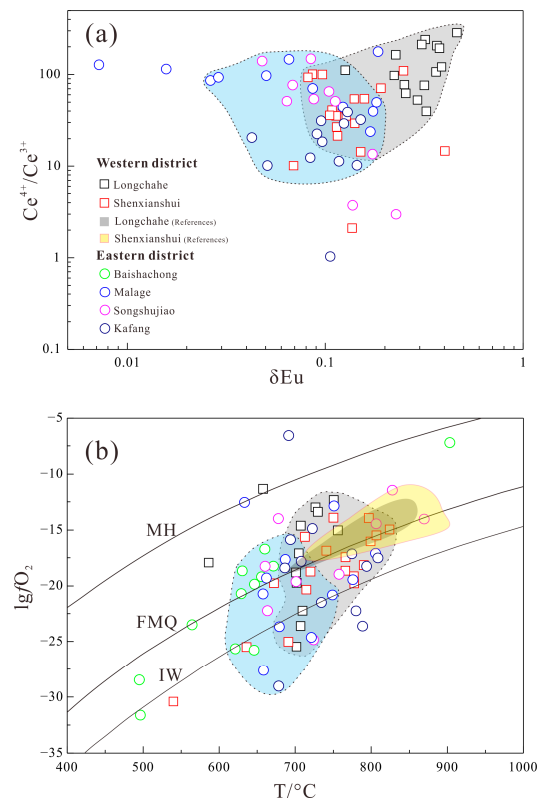


Figure 9. (a) Ce^{4+}/Ce^{3+} ratios vs. δEu , and (b) $lgfO_2$ vs. temperatures of zircons from the Gejiu ore district. Reference data come from [22].

Magma Fractionation

Tin mineralization is generally considered to be related to highly fractionated granites, which eventually enriched Sn in late magmatic-hydrothermal fluids [10,16,26]. On the whole, the negative correlations between whole-rock P_2O_5 , TiO_2 , $Mg^\#$, Sr, La/Y, δEu and SiO_2 contents indicate the possible fractionating phases were apatite, titanite, mafic minerals (e.g., biotite), and feldspars (Figure 10). In the diagram representing the evolution index (Figure 10c–f), the western district granites, especially Longchahe samples, are different from the eastern district granite, showing a low degree of fractionation. In the spider diagram (Figure 4a), the eastern district granites have more depleted Ba, Sr, P, Eu, and Ti characteristics than the western district granites. In the REE distribution diagram (Figure 4b), the eastern district granites show obvious Eu anomalies. The above chemical characteristics of the eastern district granites indicate highly evolved magmatic rocks, while those in the western district are less evolved magmatic rocks.

Previous studies have shown that some trace element pairs with similar physicochemical properties can reflect the degree of magmatic differentiation, such as Nb-Ta and Zr-Hf. Previous studies have shown that the Nb/Ta ratio decreases with magmatic differentiation [63–65], and during the late magmatic fluid interaction, Nb and Ta may be fractionated in highly evolved peraluminous granites, resulting in a decrease in the Nb/Ta ratio (less than 5) [63,66]. Therefore, fractional crystallization and hydrothermal alteration can lead to a low Nb/Ta ratio in highly evolved granitic melts. Moreover, it is suggested that the Nb/Ta ratio of ~ 5 should be used to distinguish Sn-W-bearing granites from barren-bearing granites [63,67]. Zr/Hf ratio is another effective differentiation index for granite melts.

Since zircon is the main mineral containing Zr and Hf, the crystallization of zircon will lead to the gradual depletion of Zr relative to Hf in the residual melt [64,68]. In the Nb/Ta vs. Zr/Hf diagram (Figure 11), the western district granites have higher Nb/Ta and Zr/Hf ratios than the eastern district granites, indicating relatively low magmatic differentiation, which is far away from the ore-forming granite field proposed by previous studies [63,67]. The whole-rock Rb/Sr ratio is usually used to indicate the extent of magmatic fractionation. The western district granites have higher Rb/Sr ratios than the eastern district granites, also indicating less evolved granites.

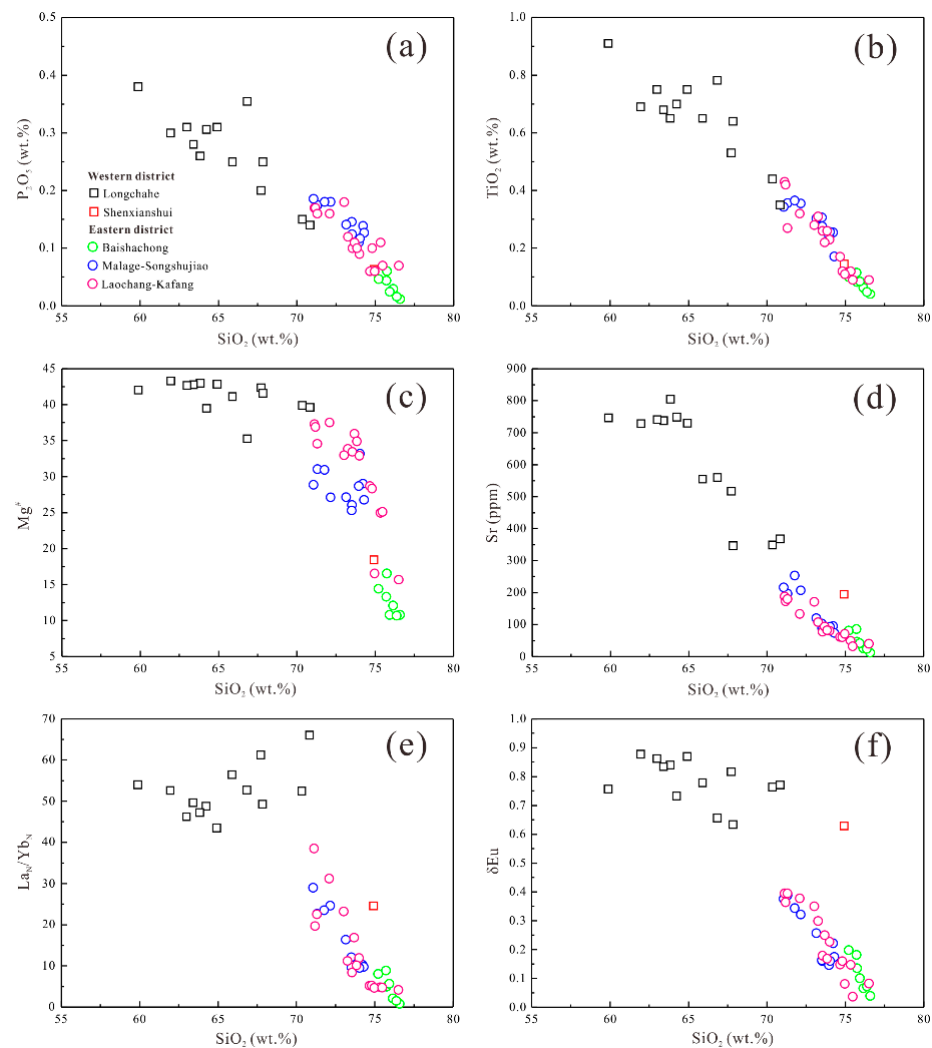


Figure 10. Selected major and trace element Harker diagrams of the granites from the Gejiu ore district (whole-rock data). (a) P_2O_5 vs. SiO_2 ; (b) TiO_2 vs. SiO_2 ; (c) $Mg^\#$ vs. SiO_2 ; (d) Sr vs. SiO_2 ; (e) La_N/Yb_N vs. SiO_2 ; (f) δEu vs. SiO_2 .

The high degree of fractionation may be due to the high F content in the magma. The experimental data show that the addition of F significantly reduces the density and viscosity of granite melt, which leads to the enhancement of crystal sedimentation [69]. Further, the increase in F in silicate melt can decrease the solidus temperature to as low as 450~550 °C (4~5 wt.% F) [69,70], which greatly prolongs the duration of magmatic fractionation. Compared with the western district granites (Figure 6c), the high F contents of micas from the eastern district granites and the widespread exposure of fluorite indicate that the eastern district granites are F-rich, which is consistent with the apatite study [71]. These are also consistent with petrographic and field observations, such as the fluorite inclusions in plagioclase and the coexistence of fluorite with cassiterite [12,17].

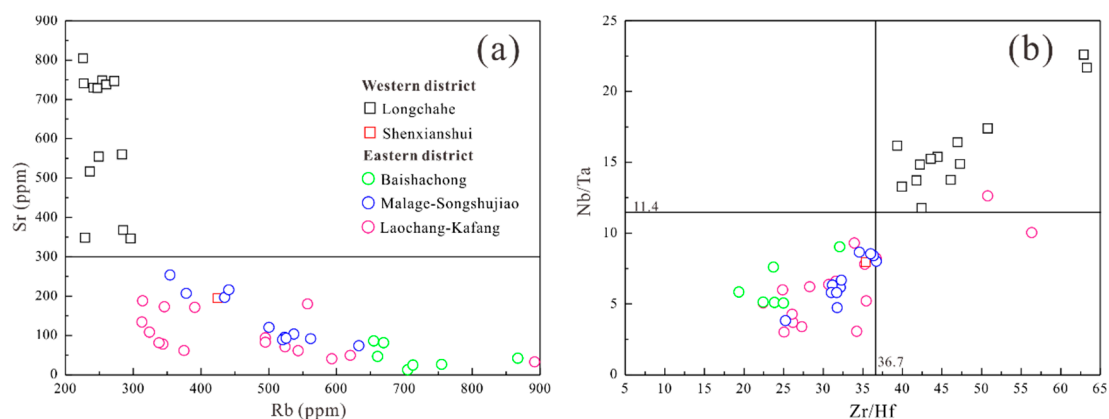


Figure 11. (a) Diagram of Rb vs. Sr, and (b) Zr/Hf vs. Nb/Ta of granites from the Gejiu ore district (whole-rock data).

Sn is an incompatible element and prefers to remain in melts during granitic magma crystallization, especially the deeper intrusions with low chlorine contents [52,72]. The Sn-bearing concealed granites from the eastern Gejiu district have high Rb/Sr ratios (Table S1) and low chlorine contents according to the chemical composition of mica (Table S4), which promoted the enrichment of tin in the granitic magma. Volatile components in reduced fractionated peraluminous magma ($fO_2 \leq Ni-NiO$ buffer) can facilitate the solubility of SnO_2 , which is conducive to the extraction and complexing of Sn [73,74]. The eastern district granites have higher Li contents (>70 ppm) than the western district granites [51], indicating that the high volatile component could improve the Sn mineralization in the Gejiu area.

Magma Temperature

Another key factor for Sn enrichment in melts is melt temperature: low-temperature melting (muscovite dehydrated melting) causes Sn enrichment in restite minerals (such as biotite), while high-temperature melting (biotite dehydrated melting) causes Sn to enter melts [45,75,76]. Previous studies have shown that the solubility of zircon in magma is sensitive to temperature and less sensitive to other parameters [77], so the crystallization temperature of magma can be estimated by the concentration of Zr in the whole rock. The melting temperature of granite melts is estimated by the zircon saturation thermometer [78]. Samples from the western granites yield slightly higher zircon saturation temperatures (754~855 °C, average of 820 °C) than the eastern granites (735~835 °C, average of 785 °C). This is consistent with the calculation results of the zircon titanium thermometer based on the SiO_2 and TiO_2 activities assumed by felsic rocks [6,24,79] (Figure 9, Table S2). Almost all of them indicate that the western granites have a slightly higher crystallization temperature, and the high-temperature melting (biotite dehydrated melting) results in the partitioning of Sn into melts [45,75,76]. However, why is there no large-scale tin deposit in the western district? First of all, the western district granites are derived from melts with more mantle-derived components and clay-poor metagraywacke sources compared with the eastern district granites, which are not conducive to large-scale mineralization. Secondly, the western district granites, having higher oxygen fugacity compared with the eastern district granites, will increase the stability of biotite and sphene, resulting in tin occurrence in the residual minerals in the source and depletion in the melt [45]. Thirdly, Sn mineralization is generally thought to be associated with highly fractionated granites, and the western district granites have less evolved than the eastern district granites. In summary, the western district granites have different magmatic sources and melting conditions from the eastern district granites, which leads to a difference in their metallogenic potential.

5.2.3. Field Observations

In addition to the ore-controlling factors of magmatic source and melting conditions, the role of sedimentary wall rocks and structural styles in the ore-forming process cannot be ignored. The exposed sedimentary rocks in the Gejiu mining area mainly belong to the Middle Triassic Gejiu Formation and Falang Formation [80]. The Gejiu Formation is composed of limestone, argillaceous limestone, and dolomite limestone, which mainly occur in the eastern district of the Gejiu mining area. The western district is mainly composed of the Falang Formation, which includes siltstone and argillaceous limestone. The rocks of the Falang Formation are deposited on the rocks of the Gejiu Formation [80]. Apart from the melting of crustal sources, the ore-bearing differences in sedimentary strata may have different contributions to W-Sn mineralization [81]. Previous studies considered that the wall-rock medium of the Gejiu Formation is enriched in organic carbon, sulfur, and the initial enrichment of corresponding metal elements (e.g., Sn), while the strata of the Middle Triassic Falang Formation do not have the above characteristics, which may lead to the difference in metallogenic potential between the eastern and western districts [82]. Middle Triassic basalts are the oldest magmatic rocks exposed in the Gejiu mining area, and Late Cretaceous intrusive rocks contain the largest amounts of magmatic rocks, ranging from gabbro to granite [22]. In the eastern district, the majority of granitic intrusions are not exposed, while the exposed area of the western district granites is about 320 km², which may lead to the denudation of tin-bearing rocks (Figure 1). Moreover, gabbro and mafic microgranular enclaves occur in the western district, indicating more mantle-derived materials than in the eastern district.

In addition to the N-S striking Gejiu Fault, there are three faults (striking E-W, NNE-SSW, and NW-SE) in the eastern district, while NNE-striking is dominated in the western district and E-W and NW-SE striking faults are rare. Xu et al. (2022) [22] showed that during the Cretaceous granite emplacement, the stress field directions on both sides of the Gejiu fault were different. In the Late Cretaceous, there is a (trans)-tensional environment to the east of the Gejiu fault and a (trans)-pressional one to the west of the fault. In general, an extensional environment has the potential to develop effective fluid channels, which may lead to large ore deposits. However, in the western district, the granite intrusive bodies were emplaced in an overall compression environment that is not conducive to hydraulic fracturing and mineralization [22].

5.3. Geodynamic Implications

The Gejiu ore district is located in the western Cathaysia Block of the South China Block, belonging to the EW-trending Late Cretaceous igneous rock and Sn-W mineralization belt in the southernmost margin of South China (Figure 12) [23,25,26]. However, there is still a dispute over whether the EW-trending Late Cretaceous magmatism and associated ore deposits were influenced by the Pacific tectonic regime or the Tethys tectonic regime [10,18]. The Pacific Plate changed its drift direction from southwest to northwest at about 125 Ma, so it is difficult to reveal the EW-trending Late Cretaceous magmatism and associated ore deposit belt [7,25,26,83]. Moreover, because the Neo-Tethys subduction zone is far away from the South China Block, its influence has not received enough attention before. Recently, more and more studies show that the South China Block was affected by both the Pacific and Neo-Tethys tectonic regimes [18,23–26,84]. Zhang et al. (2017) [25] reconstructed the palaeogeographic location of Southeast Asia by GPlates and found that the Neo-Tethys trench was close to the South China Block during the Cretaceous period. More and more studies have shown that the Neo-Tethys Plate started to subduct beneath the South China Block at about 125 Ma through flat subduction; therefore, the subducted ridge could extend far away from the subduction zone [7,23,25,83–85]. Moreover, an EW-trending Late Cretaceous igneous belt and Sn-W metallogenic belt have been identified in the southernmost margin of South China [23,25], which is parallel to the northward subduction of the Neo-Tethys Plate but perpendicular to the northwest subduction of the Paleo-Pacific Plate. According to Li et al. (2014) [28], the tectonic regime of the South China Block changed to WNW-ESE-oriented

transpression, which caused the cessation of extension-related magmatism. Considering the Late Cretaceous NS-trending extension in South China and the long distance from southwest China, we preferred the northward subduction of the Neo-Tethys Plate beneath South China as its geodynamic mechanism (Figure 12). Accordingly, the Gejiu ore district, located in the E-W metallogenic belts, should be related to the Neo-Tethys tectonic regime (Figure 12). Moreover, during the Tethyan subduction, the western granites showed higher temperatures, oxygen fugacity, and mantle-derived components than the eastern granites in the Gejiu ore district.

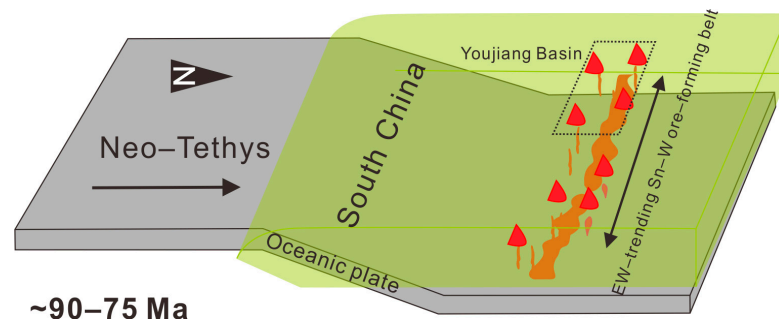


Figure 12. Schematic map illustrating the northward subduction of the Neo-Tethys plate beneath the South China Block (modified from [23]). The red triangle cones are magmatism and Sn-W deposits.

6. Conclusions

(1) Systematic LA-ICP-MS zircon U-Pb analyses of six samples from the eastern and western districts in the Gejiu ore district yielded two-period ages: the younger from 73.8 to 75.6 Ma and the older from 79.2 to 83.3 Ma. We have identified a younger phase of magmatic activity (73.8~75.6 Ma).

(2) The western district granites have higher oxygen fugacity and lower F content and magmatic differentiation than the eastern district granites, indicating that the western district granites are not conducive to mineralization. Different magmatic sources and sedimentary-structural styles also indicate differences in mineralization potential between the eastern district and the western district granites.

(3) The Gejiu ore district, located in the EW-trending Late Cretaceous granite and Sn-W metallogenic belts, was formed by the northward subduction of the Neo-Tethys Plate.

Supplementary Materials: The following supporting information can be downloaded at: <https://www.mdpi.com/article/10.3390/min13050691/s1>, Figure S1: Cathodoluminescence images of zircon grains for Gejiu ore district, and the $^{206}\text{Pb}/^{238}\text{U}$ ages of analytical spots are marked in red text. Figure S2: (a–f) Zircon chondrite-normalized REE distribution patterns of Gejiu ore district. Table S1: Sheet 1-Whole rock major (in wt.%) and trace elements (in ppm) data of granitoids from Gejiu ore district, China (This study). Sheet 2-Whole rock major (in wt.%) and trace elements (in ppm) data of granitoids from Gejiu ore district, China [10]. Sheet 3-Average Sn and Li Contents (ppm) of Gejiu igneous rocks taken from [51]. Table S2: LA-ICP-MS zircon U-Pb ages (Sheet 1) and trace elements (Sheet 2) of granitoids from Gejiu ore district, China. Table S3: LA-MC-ICP-MS zircon Hf isotopic compositions of the granite from Gejiu ore district, China. Table S4: Representative compositions and structural formula of biotite from Gejiu granite.

Author Contributions: Conceptualization, S.S. and S.L.; Data curation, S.S., J.Z. and S.L.; Funding acquisition, S.S. and W.S.; Methodology, S.S., J.Z. and H.N.; Writing—original draft preparation, S.S. and S.L.; writing—review and editing, S.S., J.Z., S.L. and Z.W. All authors have read and agreed to the published version of the manuscript.

Funding: This study is supported by the National Natural Science Foundation of China (Grant Nos. 92258303), Laoshan Laboratory (Grant Nos. LSKJ202204100) and the Strategic Priority Research Program (B) of the Chinese Academy of Sciences (Grant Nos. XDB42020303).

Data Availability Statement: All data, models, or codes that support the findings of this study are available from the corresponding author upon reasonable request.

Acknowledgments: We are grateful to Yuquan Zhang for his help during the sampling, Lorenzo Fedele and Robert Trumbull for their suggestions. We also thank three anonymous reviewers and editor for very insightful and thorough reviews.

Conflicts of Interest: The authors declare no conflict of interest.

References

1. Burnham, A.D.; Berry, A.J. Formation of Hadean granites by melting of igneous crust. *Nat. Geosci.* **2017**, *10*, 457. [\[CrossRef\]](#)
2. Che, X.D.; Linnen, R.L.; Wang, R.C.; Aseri, A.; Thibault, Y. Tungsten solubility in evolved granitic melts: An evaluation of magmatic wolframite. *Geochim. Cosmochim. Acta* **2013**, *106*, 84–98. [\[CrossRef\]](#)
3. Kelemen, P.B.; Behn, M.D. Formation of lower continental crust by relamination of buoyant arc lavas and plutons. *Nat. Geosci.* **2016**, *9*, 197–205. [\[CrossRef\]](#)
4. Linnen, R.L.; Pichavant, M.; Holtz, F. The combined effects of fO_2 and melt composition on SnO_2 solubility and tin diffusivity in haplogranitic melts. *Geochim. Cosmochim. Acta* **1996**, *60*, 4965–4976. [\[CrossRef\]](#)
5. Cerny, P.; Blevin, P.L.; Cuney, M.; London, D. Granite-related ore deposits. *Econ. Geol.* **2005**, *100*, 337–370.
6. Sun, S.J.; Yang, X.Y.; Wang, G.J.; Sun, W.D.; Zhang, H.; Li, C.Y.; Ding, X. In situ elemental and Sr-O isotopic studies on apatite from the Xu-Huai intrusion at the southern margin of the North China Craton: Implications for petrogenesis and metallogeny. *Chem. Geol.* **2019**, *510*, 200–214. [\[CrossRef\]](#)
7. Sun, W.D.; Li, S.; Yang, X.Y.; Ling, M.X.; Ding, X.; Duan, L.A.; Zhan, M.Z.; Zhang, H.; Fan, W.M. Large-scale gold mineralization in eastern China induced by an Early Cretaceous clockwise change in Pacific plate motions. *Int. Geol. Rev.* **2013**, *55*, 311–321. [\[CrossRef\]](#)
8. Burnham, C.W.; Ohmoto, H. Late-stage processes of felsic magmatism. *Min. Geol. Spec. Issue* **1980**, *8*, 1–11.
9. Lehmann, B. *Metallogeny of Tin*; Lecture Notes in Earth Sciences; Springer: Berlin/Heidelberg, Germany, 1990; Volume 32, p. 211.
10. Cheng, Y.B.; Mao, J.W. Age and geochemistry of granites in Gejiu area, Yunnan province, SW China: Constraints on their petrogenesis and tectonic setting. *Lithos* **2010**, *120*, 258–276.
11. Cheng, Y.B.; Mao, J.W.; Chang, Z.S.; Pirajno, F. The origin of the world class tin-polymetallic deposits in the Gejiu district, SW China: Constraints from metal zoning characteristics and ^{40}Ar - ^{39}Ar geochronology. *Ore Geol. Rev.* **2013**, *53*, 50–62. [\[CrossRef\]](#)
12. Cheng, Y.B.; Mao, J.W.; Rusk, B.; Yang, Z.X. Geology and genesis of Kafang Cu-Sn deposit, Gejiu district, SW China. *Ore Geol. Rev.* **2012**, *48*, 180–196. [\[CrossRef\]](#)
13. Cheng, Y.B.; Mao, J.W.; Spandler, C. Petrogenesis and geodynamic implications of the Gejiu igneous complex in the western Cathaysia block, South China. *Lithos* **2013**, *175–176*, 213–229. [\[CrossRef\]](#)
14. Cheng, Y.B.; Spandler, C.; Kemp, A.; Mao, J.W.; Rusk, B.; Hu, Y.; Blake, K. Controls on cassiterite (SnO_2) crystallization: Evidence from cathodoluminescence, trace-element chemistry, and geochronology at the Gejiu Tin District. *Am. Mineral.* **2019**, *104*, 118–129. [\[CrossRef\]](#)
15. *Geological Team of No. 308. Geology of Tin Deposit in Gejiu Area*; Metallurgical Industry Publishing House: Beijing, China, 1984; pp. 50–90. (In Chinese)
16. Guo, J.; Xiang, L.; Zhang, R.Q.; Yang, T.; Wu, K.; Sun, W.D. Chemical and boron isotopic variations of tourmaline deciphering magmatic-hydrothermal evolution at the Gejiu Sn-polymetallic district, South China. *Chem. Geol.* **2022**, *593*, 20. [\[CrossRef\]](#)
17. Guo, J.; Zhang, R.Q.; Li, C.Y.; Sun, W.D.; Hu, Y.B.; Kang, D.M.; Wu, J.D. Genesis of the Gaosong Sn-Cu deposit, Gejiu district, SW China: Constraints from in situ LA-ICP-MS cassiterite U-Pb dating and trace element fingerprinting. *Ore Geol. Rev.* **2018**, *92*, 627–642. [\[CrossRef\]](#)
18. Mao, J.W.; Xie, G.Q.; Guo, C.L.; Yuan, S.D.; Cheng, Y.B.; Chen, Y.C. Spatial-temporal distribution of Mesozoic ore deposits in South China and their metallogenic settings. *Geol. J. China Univ.* **2008**, *14*, 510–526. (In Chinese with English Abstract)
19. Zhang, J.W.; Dai, C.G.; Huang, Z.L.; Luo, T.Y.; Qian, Z.K.; Zhang, Y. Age and petrogenesis of Anisian magnesian alkali basalts and their genetic association with the Kafang stratiform Cu deposit in the Gejiu supergiant tin-polymetallic district, SW China. *Ore Geol. Rev.* **2015**, *69*, 403–416. [\[CrossRef\]](#)
20. Zhuang, Y.Q.; Wang, R.Z.; Yang, S.P. *Tin-Copper Polymetallic Deposits*; Earthquake Publishing House: Beijing, China, 1996; pp. 38–100. (In Chinese)
21. Jiang, Z.W.; Oliver, N.H.S.; Barr, T.D.; Power, W.L.; Ord, A. Numerical modeling of fault-controlled fluid flow in the genesis of tin deposits of the Malage ore field, Gejiu mining district, China. *Econ. Geol. Bull. Soc. Econ. Geol.* **1997**, *92*, 228–247. [\[CrossRef\]](#)
22. Xu, R.; Romer, R.L.; Kroner, U.; Deng, J. Tectonic control on the spatial distribution of Sn mineralization in the Gejiu Sn district, China. *Ore Geol. Rev.* **2022**, *148*, 16. [\[CrossRef\]](#)
23. Sun, S.J.; Zhang, L.P.; Zhang, R.Q.; Ding, X.; Zhu, H.L.; Zhang, Z.F.; Sun, W.D. Mid-Late Cretaceous igneous activity in South China: The Qianjia example, Hainan Island. *Int. Geol. Rev.* **2018**, *60*, 1665–1683. [\[CrossRef\]](#)
24. Sun, S.J.; Zhang, R.Q.; Cong, Y.N.; Zhang, L.P.; Sun, W.D.; Li, C.Y.; Ding, X. Analogous diagenetic conditions of dark enclave and its host granite derived by magma mixing: Evidence for a post-mixing magmatic process. *Lithos* **2020**, *356*, 12. [\[CrossRef\]](#)
25. Zhang, L.P.; Hu, Y.B.; Liang, J.L.; Ireland, T.; Chen, Y.L.; Zhang, R.Q.; Sun, S.J.; Sun, W.D. Adakitic rocks associated with the Shilu copper-molybdenum deposit in the Yangchun Basin, South China, and their tectonic implications. *Acta Geochim.* **2017**, *36*, 132–150. [\[CrossRef\]](#)

26. Zhang, L.P.; Zhang, R.Q.; Chen, Y.X.; Sun, S.J.; Liang, J.L.; Sun, W.D. Geochronology and geochemistry of the Late Cretaceous Xinpeng granitic intrusion, South China: Implication for Sn-W mineralization. *Ore Geol. Rev.* **2019**, *113*, 11. [[CrossRef](#)]
27. Zheng, Q.A.; Yang, D.S. The mineralization evolution and metallogenic model of the Gejiu tin-polymetallic deposits in Yunnan province. *Geol. Explor. Non-Ferr. Met.* **1997**, *6*, 82–87. (In Chinese with English Abstract)
28. Li, S.; Yang, X.Y.; Huang, Y.; Sun, W.D. Petrogenesis and mineralization of the Fenghuangshan skarn Cu-Au deposit, Tongling ore cluster field, Lower Yangtze metallogenic belt. *Ore Geol. Rev.* **2014**, *58*, 148–162. [[CrossRef](#)]
29. Sun, S.J.; Ireland, T.R.; Zhang, L.P.; Zhang, R.Q.; Zhang, C.C.; Sun, W.D. Palaeoarchaeic materials in the Tibetan Plateau indicated by zircon. *Int. Geol. Rev.* **2018**, *60*, 1061–1072. [[CrossRef](#)]
30. Lin, J.; Liu, Y.S.; Yang, Y.H.; Hu, Z.C. Calibration and correction of LA-ICP-MS and LA-MC-ICP-MS analyses for element contents and isotopic ratios. *Solid Earth Sci.* **2016**, *1*, 5–27. [[CrossRef](#)]
31. Ludwig, K.R. User's manual for Isoplot 3.00: A geochronological toolkit for Microsoft Excel. *Berkeley Geochronol. Cent. Spec. Publ.* **2003**, *4*, 1–70.
32. Li, X.H.; Long, W.G.; Li, Q.L.; Liu, Y.; Zheng, Y.F.; Yang, Y.H.; Chamberlain, K.R.; Wan, D.F.; Guo, C.H.; Wang, X.C.; et al. Penglai zircon megacrysts: A potential new working reference material for microbeam determination of Hf–O isotopes and U–Pb age. *Geostand. Geoanalytical Res.* **2010**, *34*, 117–134. [[CrossRef](#)]
33. Wu, F.Y.; Yang, Y.H.; Xie, L.W.; Yang, J.H.; Xu, P. Hf isotopic compositions of the standard zircons and baddeleyites used in U–Pb geochronology. *Chem. Geol.* **2006**, *234*, 105–126. [[CrossRef](#)]
34. Ma, L.H.; Cai, Y.F.; Liu, X.J.; Xu, J.F.; Zhou, Y.; Su, X.Q. Chemical Composition of Biotite from the Gejiu Granite, Yunnan Province: Implication for Petrogenesis and Mineralization of Kafang Tin Polymetallic Deposit. *Geol. J. China Univ.* **2018**, *24*, 692–701. (In Chinese with English Abstract)
35. Sun, S.S.; McDonough, W.F. Chemical and isotopic systematics of oceanic basalts: Implications for mantle composition and processes. *Geol. Soc. Lond. Spec. Publ.* **1989**, *42*, 313–345. [[CrossRef](#)]
36. Belousova, E.A.; Griffin, W.L.; Suzanne, Y.O.R.; Fisher, N.I. Igneous zircon: Trace element composition as an indicator of source rock type. *Contrib. Mineral. Petrol.* **2002**, *143*, 602–622. [[CrossRef](#)]
37. Ballard, J.R.; Palin, J.M.; Campbell, I.H. Relative oxidation states of magmas inferred from Ce(IV)/Ce(III) in zircon: Application to porphyry copper deposits of northern Chile. *Contrib. Mineral. Petrol.* **2002**, *144*, 347–364. [[CrossRef](#)]
38. Foster, M.D. Interpretation of composition of trioctahedral micas. *U.S. Geol. Surv. Prof. Pap.* **1960**, *354B*, 1–49.
39. Wones, D.R.; Eugster, H.P. Stability of biotite: Experiment, theory, and application. *Am. Mineral.* **1965**, *50*, 1228–1272.
40. Zhang, Y.C.; Chen, S.; Zhao, J.; Zhao, Y.; Li, J. Compositional characteristics and petrogenetic and metallogenic significance of biotite in granite in Gejiu tin polymetallic ore concentration area, Yunnan province. *J. Mineral. Petrol.* **2020**, *40*, 76–88. (In Chinese with English Abstract)
41. Liu, Y.B.; Zhang, L.F.; Mo, X.X.; Santosh, M.; Dong, G.C.; Zhou, H.Y. The giant tin polymetallic mineralization in southwest China: Integrated geochemical and isotopic constraints and implications for Cretaceous tectonomagmatic event. *Geosci. Front.* **2020**, *11*, 1593–1608. [[CrossRef](#)]
42. Wang, X.; Ren, M.H. Assessment of the ore-forming process of the Gejiu tin district (South China). *Ore Geol. Rev.* **2019**, *107*, 707–734. [[CrossRef](#)]
43. Chen, Y.X.; Li, H.; Sun, W.D.; Ireland, T.; Tian, X.F.; Hu, Y.B.; Yang, W.B.; Chen, C.; Xu, D.R. Generation of Late Mesozoic Qianlishan A₂-type granite in Nanling Range, South China: Implications for Shizhuyuan W–Sn mineralization and tectonic evolution. *Lithos* **2016**, *266–267*, 435–452. [[CrossRef](#)]
44. Hedenquist, J.W.; Lowenstern, J.B. The role of magmas in the formation of hydrothermal ore-deposits. *Nature* **1994**, *370*, 519–527. [[CrossRef](#)]
45. Romer, R.L.; Kroner, U. Sediment and weathering control on the distribution of Paleozoic magmatic tin-tungsten mineralization. *Miner. Depos.* **2015**, *50*, 327–338. [[CrossRef](#)]
46. Chen, B.; Zhai, M.G.; Shao, J.A. Petrogenesis and significance of the Mesozoic North Taihang complex: Major and trace element evidence. *Sci. China Ser. D Earth Sci.* **2003**, *46*, 941–953. [[CrossRef](#)]
47. Deniel, C.; Vidal, P.; Fernandez, A. Isotopic study of the Manaslu granite (Himalaya, Nepal): Inferences on the age and source of Himalayan leucogranites. *Contrib. Mineral. Petrol.* **1987**, *96*, 78–92. [[CrossRef](#)]
48. Chen, B.; Jahn, B.M.; Wilde, S.; Xu, B. Two contrasting paleozoic magmatic belts in northern Inner Mongolia, China: Petrogenesis and tectonic implications. *Tectonophysics* **2000**, *328*, 157–182. [[CrossRef](#)]
49. Hildreth, W.; Moorbath, S. Crustal contributions to arc magmatism in the Andes of Central Chile. *Contrib. Mineral. Petrol.* **1988**, *98*, 455–489. [[CrossRef](#)]
50. Yang, J.H.; Zhou, M.F.; Hu, R.Z.; Zhong, H.; Williams-Jones, A.E.; Liu, L.; Zhang, X.C.; Fu, Y.Z.; Mao, W. Granite-Related Tin Metallogenic Events and Key Controlling Factors in Peninsular Malaysia, Southeast Asia: New Insights from Cassiterite U–Pb Dating and Zircon Geochemistry. *Econ. Geol.* **2020**, *115*, 581–601. [[CrossRef](#)]
51. Zhang, H.P.; Liu, J.S.; Li, X.B.; Zhang, X.L. Relationship of granites to tin, silver, copper, lead, zinc, polymetallic deposits in southeastern Yunnan, China. *Contrib. Geol. Miner. Resour. Res.* **2006**, *21*, 87–90. (In Chinese with English Abstract)
52. Gomes, M.E.P.; Neiva, A.M.R. Petrogenesis of tin-bearing granites from Ervedosa, Northern Portugal: The importance of magmatic process. *Chem. Erde/Geochem.* **2002**, *62*, 47–72. [[CrossRef](#)]
53. Sylvester, P.J. Post-collisional strongly peraluminous granites. *Lithos* **1998**, *45*, 29–44. [[CrossRef](#)]

54. Yi, W.; Halliday, A.N.; Alt, J.C.; Lee, D.C.; Rehkamper, M.; Garcia, M.O.; Su, Y.J. Cadmium, indium, tin, tellurium, and sulfur in oceanic basalts: Implications for chalcophile element fractionation in the Earth. *J. Geophys. Res. -Solid Earth* **2000**, *105*, 18927–18948. [[CrossRef](#)]
55. Linnen, R.L.; Pichavant, M.; Holtz, F.; Burgess, S. The effect of fO_2 source on the solubility, diffusion, and speciation of tin in haplogranitic melt at 850°C and 2 kbar. *Geochim. Cosmochim. Acta* **1995**, *59*, 1579–1588. [[CrossRef](#)]
56. Thompson, J.F.H.; Sillitoe, R.H.; Baker, T.; Lang, J.R.; Mortensen, J.K. Intrusion related gold deposits associated with tungsten-tin provinces. *Miner. Depos.* **1999**, *34*, 323–334. [[CrossRef](#)]
57. Blevin, P.L. Redox and compositional parameters for interpreting the granitoid metallogeny of eastern Australia: Implications for gold-rich ore systems. *Resour. Geol.* **2004**, *54*, 241–252. [[CrossRef](#)]
58. Ishihara, S. The redox state of granitoids relative to tectonic setting and earth history: The magnetite–ilmenite series 30 years later. *Trans. R. Soc. Edinb. Earth Sci.* **2004**, *95*, 23–33.
59. Lehmann, B.; Mahawat, C. Metallogeny of tin in central Thailand—A genetic concept. *Geology* **1989**, *17*, 426–429. [[CrossRef](#)]
60. Barrière, M.; Cotton, J. Biotites and associated minerals as markers of magmatic fractionation and deuteritic equilibration in granites. *Contrib. Mineral. Petrol.* **1979**, *70*, 183–192. [[CrossRef](#)]
61. Wones, D.R. Significance of the assemblage titanite+magnetite+quartz in granitic rocks. *Am. Mineral.* **1989**, *74*, 744–749.
62. Richards, J.P.; Engr, C. Did Paleo-Tethyan anoxia kill arc magma fertility for porphyry copper formation? *Geology* **2017**, *45*, G38954.1. [[CrossRef](#)]
63. Ballouard, C.; Branquet, Y.; Tartese, R.; Poujol, M.; Boulvais, P.; Vigneresse, J.L. Nb-Ta fractionation in peraluminous granites: A marker of the magmatic-hydrothermal transition. *Geology* **2016**, *44*, 231–234. [[CrossRef](#)]
64. Chen, J.Y.; Yang, J.H. Petrogenesis of the Fogang highly fractionated I-type granitoids: Constraints from Nb, Ta, Zr and Hf. *Acta Petrol. Sin.* **2015**, *31*, 846–854.
65. Linnen, R.L.; Keppler, H. Columbite solubility in granitic melts: Consequences for the enrichment and fractionation of Nb and Ta in the Earth's crust. *Contrib. Mineral. Petrol.* **1997**, *128*, 213–227. [[CrossRef](#)]
66. Dostal, J.; Chatterjee, A.K. Contrasting behaviour of Nb/Ta and Zr/Hf ratios in a peraluminous granitic pluton (Nova Scotia, Canada). *Chem. Geol.* **2000**, *163*, 207–218. [[CrossRef](#)]
67. Yuan, S.D.; Williams-Jones, A.E.; Mao, J.W.; Zhao, P.L.; Yan, C.; Zhang, D.L. The origin of the Zhangjialong tungsten deposit, south china: Implications for w-sn mineralization in large granite batholiths. *Econ. Geol.* **2018**, *113*, 1193–1208. [[CrossRef](#)]
68. Zaraisky, G.; Aksyuk, A.; Devyatova, V.; Udoratina, O.; Chevychelov, V. Zr/Hf ratio as an indicator of fractionation of rare-metal granites by the example of the Kukulbei complex, eastern Transbaikalia. *Petrology* **2008**, *16*, 710–736. [[CrossRef](#)]
69. Dingwell, D.B.; Scarfe, C.M.; Cronin, D.J. The effect of fluorine on viscosities in the system $Na_2O-Al_2O_3-SiO_2$ —implications for phonolites, trachytes and rhyolites. *Am. Mineral.* **1985**, *70*, 80–87.
70. Manning, D.A.C. The effect of fluorine on liquidus phase-relationships in the system qz-ab-or with excess water at 1-kb. *Contrib. Mineral. Petrol.* **1981**, *76*, 206–215. [[CrossRef](#)]
71. Li, J.; Chen, S.Y.; Zhao, Y.H. Trace elements in apatite from Gejiu Sn polymetallic district: Implications for petrogenesis, metallogenesis and exploration. *Ore Geol. Rev.* **2022**, *145*, 16. [[CrossRef](#)]
72. Hong, W.; Cooke, D.R.; Huston, D.L.; Maas, R.; Meffre, S.; Thompson, J.; Zhang, L.J.; Fox, N. Geochronological, geochemical and Pb isotopic compositions of Tasmanian granites (southeast Australia): Controls on petrogenesis, geodynamic evolution and tin mineralisation. *Gondwana Res.* **2017**, *46*, 124–140. [[CrossRef](#)]
73. Bhalla, P.; Holtz, F.; Linnen, R.L.; Behrens, H. Solubility of cassiterite in evolved granitic melts: Effect of T, fO_2 , and additional volatiles. *Lithos* **2005**, *80*, 387–400. [[CrossRef](#)]
74. Cooke, D.R.; Kitto, P.A.; Harris, A.C.; Chang, Z.; Wilkinson, J.J.; Wilkinson, C.C.; Hollings, P.; Webster, J.D. Magma fertility and mineralisation. Smart Science for Exploration and Mining—Proceedings of the 10th Biennial SGA Meeting, Townsville. *Econ. Geol. Res. Unit* **2009**, *1*, 8–10.
75. Wolf, M.; Romer, R.L.; Franz, L.; Lopez-Moro, F.J. Tin in granitic melts: The role of melting temperature and protolith composition. *Lithos* **2018**, *310*, 20–30. [[CrossRef](#)]
76. Yuan, S.D.; Williams-Jones, A.E.; Romer, R.L.; Zhao, P.L.; Mao, J.W. Protolith-related thermal controls on the decoupling of sn and w in sn-w metallogenic provinces: Insights from the Nanling region, China. *Econ. Geol.* **2019**, *114*, 1005–1012. [[CrossRef](#)]
77. Miller, C.F.; McDowell, S.M.; Mapes, R.W. Hot and cold granites? Implications of zircon saturation temperatures and preservation of inheritance. *Geology* **2003**, *31*, 529–532. [[CrossRef](#)]
78. Watson, E.B.; Harrison, T.M. Zircon saturation revisited: Temperature and composition effects in a variety of crustal magma types. *Earth Planet. Sci. Lett.* **1983**, *64*, 295–304. [[CrossRef](#)]
79. Ferry, J.M.; Watson, E.B. New thermodynamic models and revised calibrations for the Ti-in-zircon and Zr-in-rutile thermometers. *Contrib. Mineral. Petrol.* **2007**, *154*, 429–437. [[CrossRef](#)]
80. Chen, J.; Halls, C.; Stanley, C.J. Mineral association and mineralogical criteria for the formation condition of a B-F-Sn-Bi skarn in Damoshan, Gejiu tin field. Southwest China. *Chin. J. Geochem.* **1992**, *11*, 140–155. [[CrossRef](#)]
81. Li, S.R.; Tan, J.; Deng, J. Ore types of tungsten poly-metallic deposits and prospecting indications. *China Tungst. Indust.* **2007**, *22*, 19–24. (In Chinese with English Abstract)
82. Gai, C.K. The geochemistry of wallrock medium metallogenesis of Gejiu Sn ore field. *Yunnan Geol.* **2007**, *26*, 277–283. (In Chinese)

83. Sun, W.D.; Ding, X.; Hu, Y.H.; Li, X.H. The golden transformation of the Cretaceous plate subduction in the west Pacific. *Earth Planet. Science Lett.* **2007**, *262*, 533–542. [[CrossRef](#)]
84. Sun, W.D. Initiation and evolution of the South China Sea: An overview. *Acta Geochim.* **2016**, *35*, 215–225. [[CrossRef](#)]
85. Espurt, N.; Funicello, F.; Martinod, J.; Guillaume, B.; Regard, V.; Faccenna, C.; Brusset, S. Flat subduction dynamics and deformation of the South American plate: Insights from analog modeling. *Tectonics* **2008**, *27*, 1–19. [[CrossRef](#)]

Disclaimer/Publisher’s Note: The statements, opinions and data contained in all publications are solely those of the individual author(s) and contributor(s) and not of MDPI and/or the editor(s). MDPI and/or the editor(s) disclaim responsibility for any injury to people or property resulting from any ideas, methods, instructions or products referred to in the content.